NJC

PAPER

View Article Online
View Journal

Cite this: DOI: 10.1039/c8nj02965b

Carbon dioxide electrolysis and carbon deposition in alkaline-earth-carbonate-included molten salts electrolyzer

Zhida Li, [a] Yanyan Yu, [a] Wei Li, *[b] Guanzhong Wang, [a] Li Peng, [a] Jinlian Li, [a] Di Gu, [a] Dandan Yuan [a] and Hongjun Wu *[a]

The electrochemical reduction of CO_2 in molten carbonates provides a comprehensive solution to end the detrimental global climate change, and convert and store conventional electricity in a stable chemical mode. In this work, we provide experimental validation of carbon deposition in $CaCO_3$-, $SrCO_3$- and $BaCO_3$-dissolved electrolytes. Carbon products aggregate on the cathodic surface and are then collected and characterized by electron dispersive spectroscopy (EDS), thermogravimetric analysis (TGA), scanning electron microscopy (SEM), Brunauer–Emmett–Teller (BET) surface area analysis, and X-ray diffraction (XRD) analysis. The results demonstrate that the alkaline earth carbonate additives sustain continuous CO_2 electrolysis and carbon electro-deposition. However, the micromorphology and microstructure of the carbon deposits are found to be significantly changed mainly because of the interface modification induced by the alkaline earth carbonate additives. In addition, a high yield of carbon nanotubes is observed in the cathodic carbon products by optimizing the electrolytic conditions. Compared to pure Li_2CO_3, alkaline earth carbonate additives provide carbon nanotubes with a thicker diameter and more prominent hollow structure.

Received 14th June 2018,
Accepted 13th August 2018

DOI: 10.1039/c8nj02965b

rsc.li/njc

Introduction

The worldwide awareness of the link between the global climate change and the ever-increasing carbon dioxide (CO_2) accumulation in the atmosphere has driven extensive investigations in tackling the increase in CO_2 emissions. Nevertheless, fossil fuels are still being widely utilized to meet the energy demand of human society, and therefore, the rise in CO_2 emissions will continue in the coming decades. The strategy of CO_2 capture and storage (CCS)[1,2] has already entered the view of scientific community, where CO_2 is expected to be stored in an appropriate geological stratification safely. However, in addition to being a kind of greenhouse gas, CO_2 is also a significant carbon source abundant in nature. Varying carbon dioxide capture and conversion (CCC) approaches such as chemical conversion, photochemical conversion and biological conversion have been proposed in order to create value out of wasted CO_2 exhaust and close the present carbon cycle.[3]

Electrochemical reduction of carbonate ions (CO_3^{2-}) to deposit solid carbon is a proven method that can be dated back to the mid-1960s.[4,5] Recently, this technology has received renewed interest largely due to the high necessity to reduce atmospheric CO_2 levels and avoid detrimental climate change. The molten carbonate electrolyte that is suitable to deposit carbon products from CO_2 should be able to dissolve O^{2-} (which is an intermediate product of carbon electro-deposition) and in turn help to dissolve atmospheric CO_2 and convert it into CO_3^{2-}.[6,7] Alkali carbonates of Li_2CO_3, Na_2CO_3, K_2CO_3, and particularly their mixture are the most used electrolysis media due to their properties of wide electrochemical window, rapid reaction kinetics, less corrosion ability towards anode, *etc.*[6,8,9] Ijije *et al.* established an electrolyzer with Li_2CO_3–K_2CO_3 binary melts (mole ratio: 62 : 38) under CO_2 or mixed N_2 and CO_2 atmospheres at 3.0–5.0 V and 540–700 °C, in which amorphous and various carbon nanostructures derived from dissolved CO_2 were deposited onto a mild steel cathode.[10] More recently, our group studied a Li_2CO_3–Na_2CO_3–K_2CO_3 ternary eutectic (61 : 22 : 17 by wt) and interestingly, unique porous honeycomb-like carbon and carbon nanotubes were synthesized in this molten salt environment, arousing a further interest in this domain.[11] Furthermore, carbon electro-deposition is also observed to proceed in chloride/carbonate or fluoride/carbonate mixtures as long as Li^+ is present. For example, a molten salts-electrolyzer of $CaCl_2$–$CaCO_3$–LiCl–KCl successfully achieved the electrochemical reduction of CO_2 to carbon products, where the chlorides acted as the fluxing

[a] Provincial Key Laboratory of Oil & Gas Chemical Technology, College of Chemistry & Chemical Engineering, Northeast Petroleum University, Daqing 163318, China. E-mail: hjwu@nepu.edu.cn; Tel: +86-0459-6503331
[b] College of Petroleum Engineering, Northeast Petroleum University, Daqing, 163318, China. E-mail: cyyping@sina.com; Tel: +86-0459-6504498

agent to lower the melting point of this electrolyte.[6] In addition, tetravalent CO_2 reduction into zerovalent solid carbon was fulfilled in LiF–NaF–Na_2CO_3 eutectic and in this electrolyte, CO_3^{2-} was confirmed to be regenerated from the combination between CO_2 and O^{2-}.[12]

CO_2 capture and conversion based on the molten salt–electrolysis was mostly performed in alkali carbonates previously, but relevant thermodynamic calculations show that carbon electrodeposition in alkaline earth carbonates is also possible.[6] As a supporting example, $BaCO_3$ had been employed to stabilize the molten carbonate electrolyzer due to the lower Lewis basicity of BaO than Li_2O, Na_2O and K_2O, and the nickel loss was significantly reduced during the electrolysis process.[13,14] When synthesizing carbon nanotubes *via* molten carbonate electrolysis, dissolving a certain amount of $BaCO_3$ additive in molten Li_2CO_3 generated a high yield of valued carbon nanotubes as in the pure Li_2CO_3 case.[11] However, up to now, few systematic studies of carbon production in alkaline-earth-carbonate-included molten salts have been performed. Herein, a Li_2CO_3–Na_2CO_3–K_2CO_3–MCO_3 (M = Ca, Sr, Ba) electrolyzer was fabricated to convert CO_2 into energetic carbon deposits, and the amount of MCO_3 is regulated from 0% to 30% in order to investigate the effect of alkaline earth carbonate fraction on the carbon generation process. Additionally, electrolysis in Li_2CO_3, Li_2CO_3–$CaCO_3$, Li_2CO_3–$SrCO_3$ and Li_2CO_3–$BaCO_3$ at over 700 °C was also performed, and carbon nanotubes become the preferable carbon products instead of other products.

Experimental

Battery-grade anhydrous Li_2CO_3 was provided by the Lithium Company of Shanghai, China. Na_2CO_3, K_2CO_3, $CaCO_3$ and $BaCO_3$ were of analytical purity and supplied by BA Chemical Reagent Factory of Tianjin, China. Analytically pure $SrCO_3$ was purchased from the FC Chemical Reagent Factory of Tianjin, China. A 4 cm^2 nickel plate and a galvanized iron plate were employed as the anode and cathode, respectively. A corundum crucible of 50 mL volume served as the electrolysis container. Initially, 15 g Li_2CO_3, 15 g Na_2CO_3 and 15 g K_2CO_3 were mixed and melted in a well-type crucible furnace. Then, 0% (0 g), 10% (4.5 g), 20% (9 g) and 30% (13.5 g) alkaline earth carbonate was dissolved in the Li_2CO_3–Na_2CO_3–K_2CO_3 ternary eutectic. $CaCO_3$, $SrCO_3$ and $BaCO_3$ melt at 1339 °C, 1700 °C and 1740 °C, respectively; therefore, further increasing their fraction would result in low fluidity. After heating to the presupposed temperature of 600 °C and stabilizing for 30 min, a constant current density of 250 mA cm^{-2} was applied and the electrolysis was performed for 60 min. In addition to conventional electricity, the energy consumption by melting the carbonate electrolyte and reducing the carbonate ions (CO_2) could be supplied by a sustainable solar source, which has been stated in the STEP (solar thermal electrochemical production) process.[15,16] Then, the galvanized iron plate covered by a thick layer of carbon products was pulled out from the carbonate melts and cooled at room temperature. The carbon deposits were washed with sufficient hydrochloric acid (6 M) to remove the frozen electrolyte attached on the carbon surface. Subsequent to ultrasonic treatment, filtration, washing with ultrapure water and desiccation in an air drying oven, the purified carbon powders were collected and characterized by energy dispersive spectroscopy (EDS, X-Max, the British Oxford Instruments Co., Ltd), scanning electron microscope (SEM, SIGMA, Zeiss company), thermal gravimetric analyzer (TGA, SDT-Q600, TA Instruments), Brunauer–Emmett–Teller analysis instrument (BET, Tristar-3020, Micromeritics Instrument Corporation) and X-ray diffractometer (XRD, D/MAX 2200, Rigaku).

High temperature electrolysis at over 700 °C in Li_2CO_3 and moderate amount (such as 10% by wt) of $CaCO_3$-, $SrCO_3$-, and $BaCO_3$-dissolved Li_2CO_3 was subsequently performed. The shape and area of the electrodes were changed by using a 5 cm^2 galvanized iron wire disk as the cathode and a 10 cm^2 nickel wire disk as the anode. In this case, pre-electrolysis with low current density (6 mA cm^{-2} for 15 min, 10 mA cm^{-2} for 15 min and 20 mA cm^{-2} for 5 min) was performed in order to control the growth of nickel nanoparticles on the cathodic surface. It should be noted that the described current densities are in terms of the cathode active area. The corresponding carbon products were subjected to the same purification procedures as the experiments performed at 600 °C and then, they were characterized by transmission electron microscopy (TEM, JEM-2100, JEOL).

Results and discussion

Carbon products aggregate on the cathode surface when electrolyzing the carbonate eutectic, and the digital photos of the galvanized iron plate cathode subsequent to electrolysis in Li_2CO_3–Na_2CO_3–K_2CO_3, 30% $CaCO_3$-, 30% $SrCO_3$- and 30% $BaCO_3$-included electrolyte are displayed in Fig. 1a. As is evidently illustrated, the Li_2CO_3–Na_2CO_3–K_2CO_3–$CaCO_3$ system deposits a much thicker carbon product than the other electrolyte systems. This matches well with the higher voltage plots as 30% $CaCO_3$ is dissolved in Li_2CO_3–Na_2CO_3–K_2CO_3 induced by the poor conductivity of molten $CaCO_3$ (Fig. 2a).

EDS analysis is employed to reveal the elemental composition of the purified carbon products. As shown in Fig. 1b–e, C, O, Ni, Au and Cl are present in the EDS spectrum. Au derives from the coating operation for SEM-EDS analysis; Cl is attributed to the acid leaching with hydrochloric acid; and the presence of Ni is caused by nickel oxide dissolution in the molten carbonates. Oxygen was previously investigated by Fourier transformed infrared (FTIR) spectroscopy, and the absorption peak located at 1110 cm^{-1} induced by C–C–O stretching vibration indicated the presence of oxygen-containing functional groups.[17,18] This is common for active carbons and is believed to be favorable for capacitance behavior.[19,20] Content of O, Ni, Au and Cl in each sample is very low, while C comprises an overwhelming mole fraction of over 90%. Carbon products formed in the above four systems are further studied by TGA to reveal the thermal oxidation temperature, as presented in Fig. 1f. The initial minor mass loss before 350 °C is because of the release of volatile matter, such as the residual moisture in the carbon products.

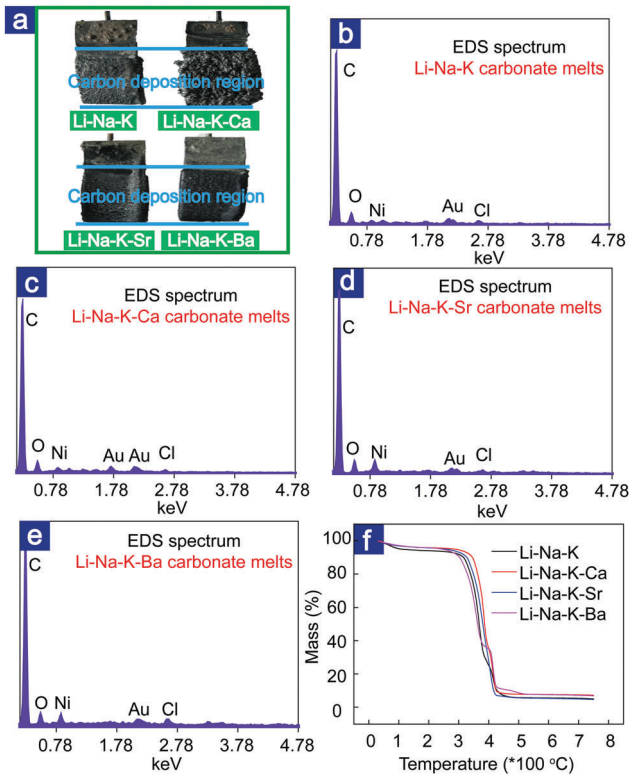

Fig. 1 (a) Images of the galvanized iron plate cathode subsequent to molten carbonate electrolysis; (b–e) EDS spectrum of the electro-deposited carbon products; (f) thermogravimetric analysis of the carbon products.

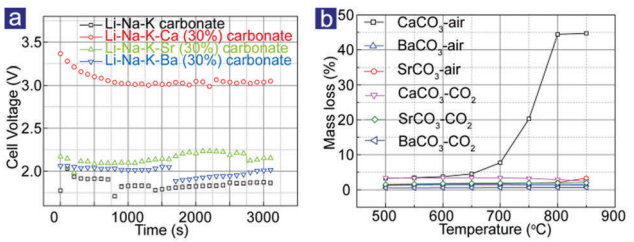

Fig. 2 (a) Cell voltage plots recorded during the electrolysis process; (b) thermogravimetric analysis of $CaCO_3$, $SrCO_3$ and $BaCO_3$ under an open air or CO_2 atmosphere.

Afterwards, a sharp mass loss occurs at 350–400 °C agreeing well with the thermal oxidation temperature of amorphous carbon in atmosphere but lower than that of carbon nanotubes and carbon spheres reported by our group.[17] After heating to 450 °C, nearly nothing is left, suggesting that the carbon products are mainly carbon plus some oxygen-containing functional groups, and this is consistent with the EDS spectrum.

Fig. 2a depicts the cell voltage recorded by the electrochemical workstation during the galvanostatic electrolysis process. The cell voltage of Li_2CO_3–Na_2CO_3–K_2CO_3 electrolysis is lower than 2.0 V, while the inclusion of alkaline earth carbonates provides a visible increase in the recorded cell voltage due to the poor conductivity of molten $CaCO_3$, $SrCO_3$ and $BaCO_3$. In particular, the inclusion of 30% $CaCO_3$ in the Li_2CO_3–Na_2CO_3–K_2CO_3 presents a cell voltage of over 3.0 V, which is higher than that obtained using Li_2CO_3–Na_2CO_3–K_2CO_3–$SrCO_3$ and Li_2CO_3–Na_2CO_3–K_2CO_3–$BaCO_3$ electrolytes. This high cell voltage, in turn, could be used to explain the observation of thicker carbon deposits (Fig. 1a).

The observed carbon deposition could be attributed to the direct splitting of molten carbonates (eqn (1)).[7,21] The intermediate metal oxides act as efficient absorbent for atmospheric CO_2 and tend to reform the carbonate electrolyte (eqn (2)). For example, the combination between Li_2O and CO_2 greenhouse gas has already been proven *via* a thermogravimetric method.[22] As presented in the indicated literature, a visible mass loss was presented when heating Li_2CO_3 up to 950 °C under an open atmosphere due to thermal decomposition (eqn (3)), but no significant mass loss was observed when CO_2 was injected or excess Li_2O was added under the same temperature. In the latter case, the reverse reaction of excess CO_2 and dissolved Li_2O to form Li_2CO_3 occurred and contributed to the decrease in mass loss (eqn (4)). We inferred that this is also the case for the alkaline earth carbonate $CaCO_3$ (Fig. 2b). Before 600 °C, no visible mass loss is observed, but then an exponential increase is present after heating to over 700 °C. This mass loss is caused by the decomposition of $CaCO_3$ into CaO and CO_2 (eqn (5)). When heated under CO_2 atmosphere, the mass loss of $CaCO_3$ is lower than 5%, which could be explained by the classical physical chemistry theory that $CaCO_3$ decomposition proceeds only when the equilibrium partial pressure of CO_2 is higher than that of the atmosphere. Compared to $CaCO_3$, $SrCO_3$ and $BaCO_3$ exhibit enhanced thermal endurance, and their mass loss is lower than 5%, under either air atmosphere or CO_2 atmosphere. The polarization ability of the central cation could explain the strengthened thermal stability of $SrCO_3$ and $BaCO_3$ compared to $CaCO_3$. For alkaline earth carbonates, carbonate ion provides a large radius; therefore, the stronger the polarization of the central cations, the greater would be the value of Z/R (Z and R represent cationic charge number and cationic radius, respectively) and more possible it is to take O^{2-} to form metal oxides and release CO_2 into the atmosphere. In this manner, the stronger polarization of Ca^{2+} makes $CaCO_3$ decompose at a relatively lower temperature than $SrCO_3$ or $BaCO_3$.

$$MCO_3(l) \rightarrow MO(l) + C(s) + O_2(g) \quad (1)$$

$$MO(l) + CO_2(g) \rightarrow MCO_3(l) \quad (2)$$

(In eqn (1) and (2), M represents Li_2, Na_2, K_2, Ca, Sr and Ba.)

$$Li_2CO_3(l) \rightarrow Li_2O(l) + CO_2(g) \quad (3)$$

$$Li_2O(l) + CO_2(g) \rightarrow Li_2CO_3(l) \quad (4)$$

$$CaCO_3(s) \rightarrow CaO(s) + CO_2(g) \quad (5)$$

Typical SEM image of the carbon products prepared by molten Li_2CO_3–Na_2CO_3–K_2CO_3 electrolysis is shown in Fig. 3. Porous, honeycomb-like carbon structure with a diameter of 300 to 500 nm is presented, and its BET surface area is quantified as 193 $m^2\ g^{-1}$, as listed in Table 1. The formation of honeycomb-like nanostructured carbon materials might be caused by rapid carbon deposition as well as the co-deposition of alkali metals.[18] Porous carbon nanostructures with large BET

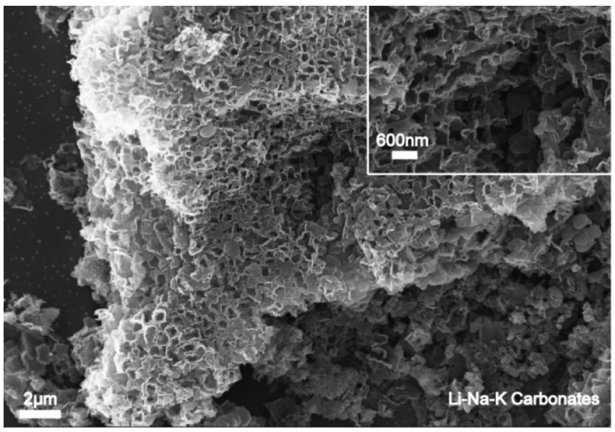

Fig. 3 Micromorphology of the carbon products electro-deposited in the Li_2CO_3–Na_2CO_3–K_2CO_3 system at 600 °C.

Table 1 BET surface areas of the carbon products deposited in various electrolyte compositions

Electrolyte	BET surface area (m^2 g^{-1})
Li–Na–K	193
Li–Na–K–Ca (10%, wt)	82
Li–Na–K–Ca (20%, wt)	85
Li–Na–K–Ca (30%, wt)	264
Li–Na–K–Sr (10%, wt)	53
Li–Na–K–Sr (20%, wt)	62
Li–Na–K–Sr (30%, wt)	76
Li–Na–K–Ba (10%, wt)	44
Li–Na–K–Ba (20%, wt)	76
Li–Na–K–Ba (30%, wt)	92

surface area demonstrate brilliant application potential in the adsorption, separation, and even catalytic conversion of CO_2.[23] Two approaches to increase the BET surface area are (i) decreasing the electrolytic temperature and (ii) increasing the applied cell voltage or current density. As a supporting example, the BET surface area of the carbon products subsequent to molten Li_2CO_3–Na_2CO_3–K_2CO_3 electrolysis with 100 mA cm^{-2} current density increases from 194 m^2 g^{-1} at 550 °C to 440 m^2 g^{-1} at 450 °C.[13] In addition, under the same electrolysis temperature of 600 °C, Li_2CO_3–Na_2CO_3 binary system electrolysis generates carbon products with a BET surface area of 39.9 m^2 g^{-1} at 50 mA cm^{-2}, which increases to 80.3 m^2 g^{-1} when the current density is enlarged to 200 mA cm^{-2}.[24] Thus, the Li_2CO_3–Na_2CO_3 binary system is expected to synthesize carbon materials with tunable BET surface area *via* the regulation of electrolytic parameters of temperature, current density, cell voltage, *etc.*

Fig. 4 depicts the carbon products acquired from $CaCO_3$-included molten carbonate electrolysis. When 10% $CaCO_3$ is dissolved in Li_2CO_3–Na_2CO_3–K_2CO_3 eutectic, a mixture of flake-like carbon and irregular carbon particles is presented in the cathodically generated carbon products, as evident in Fig. 4a and b. Upon further increasing the $CaCO_3$ mass fraction to 20%, as illustrated by Fig. 4c and d, the carbon deposits comprise carbon flakes and quasi carbon sphere clusters. Interestingly, when 30% $CaCO_3$ is dissolved in Li_2CO_3–Na_2CO_3–K_2CO_3 melts, irregular carbon particles are still formed, but the carbon flakes observed in carbonate eutectic dissolving 10% and 20% $CaCO_3$ (Fig. 4a–d) evolve into broken carbon pieces instead. Agreeing well with SEM data, the BET surface area of the carbon products is found to increase to 264 m^2 g^{-1} when 30% $CaCO_3$ is included, which is higher than that obtained using Li_2CO_3–Na_2CO_3–K_2CO_3–$CaCO_3$ (10% and 20%) and Li_2CO_3–Na_2CO_3–K_2CO_3 systems. Unlike alkali oxides, CaO deriving from the decomposition of $CaCO_3$ is nearly insoluble in molten carbonate electrolyte.[14] Moreover, the intermediate CaO is denser than molten carbonate and tends to deposit on the cathode or the bottom of the cell, of which the deposition on the iron plate cathode provides an opportunity to substantially modify the interface between the iron cathode and molten carbonate electrolyte. Carbon deposition occurs in this unusual high CaO environment, and the observed morphological evolution along with elevated $CaCO_3$ fraction is presumably induced in this manner. We have demonstrated in a previous report the morphological evolution between carbon nanotubes and quasi carbon spheres at 750 °C, where the quasi carbon spheres are synthesized in $CaCO_3$-included carbonate electrolyte, while the exclusion of $CaCO_3$ from the electrolyte provides higher carbon nanotubes fraction in the cathodic carbon products.[17] It is therefore concluded that $CaCO_3$ additive significantly influences the micromorphology and microstructure of the cathodic carbon deposits because of the nearly insoluble CaO deriving from $CaCO_3$ decomposition.

Fig. 5 shows the representative SEM images of the carbon products synthesized in $SrCO_3$-included molten carbonate electrolyte. The carbon products shown in Fig. 5a and b were synthesized in 10% $SrCO_3$ additive dissolved carbonate eutectic; those shown in Fig. 5c and d were synthesized in 20% $SrCO_3$ additive dissolved

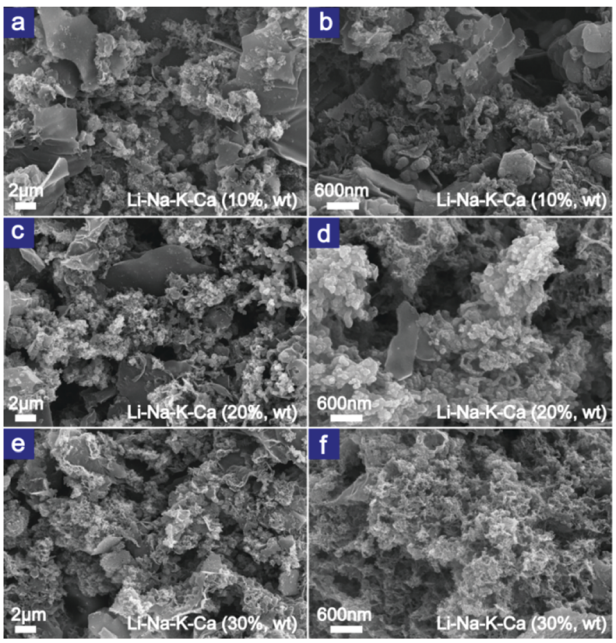

Fig. 4 Micromorphology of the carbon products subsequent to $CaCO_3$-included carbonate melts electrolysis at 600 °C.

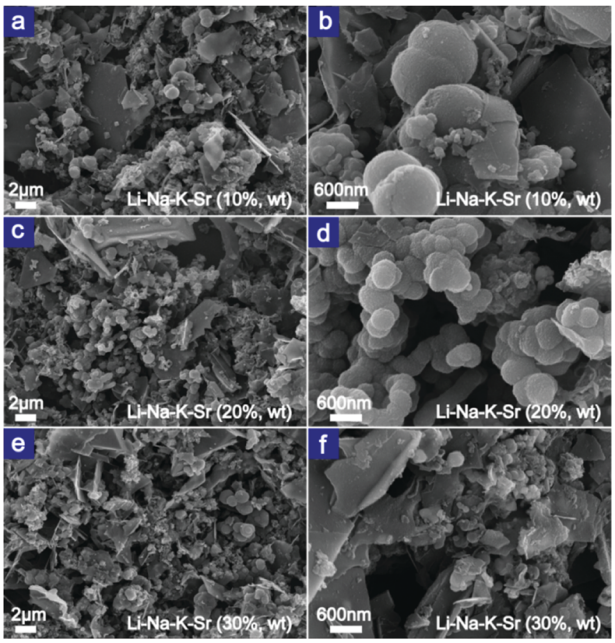

Fig. 5 Micromorphology of the carbon products deriving from $SrCO_3$-included carbonate melts electrolysis at 600 °C.

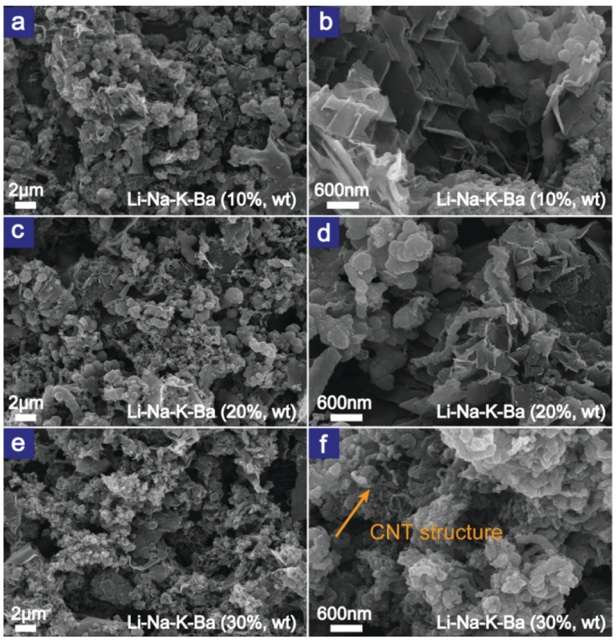

Fig. 6 Micromorphology of the carbon products deriving from $BaCO_3$-included carbonate melts electrolysis at 600 °C.

carbonate eutectic; and those shown in Fig. 5e and f were synthesized in 30% $SrCO_3$ additive dissolved carbonate eutectic. A common feature of the cathodically deposited carbon products is the presence of carbon flakes and sphere-like carbons as $SrCO_3$ was dissolved in the Li_2CO_3–Na_2CO_3–K_2CO_3 melts. In addition, due to the absence of porous carbon structure and the presence of compact flake-like and sphere-like structure, the BET surface areas of the carbon products are lower than 100 $m^2\ g^{-1}$, signifying a visible decrease compared to 193 $m^2\ g^{-1}$ of the products obtained from molten Li_2CO_3–Na_2CO_3–K_2CO_3 electrolysis (Table 1). However, it is found that with the increase in the $SrCO_3$ mass fraction, the BET surface area tends to elevate. This trend indicates an interesting phenomenon where the $SrCO_3$ additive favors compact carbon products deposition within the Li_2CO_3–Na_2CO_3–K_2CO_3 system, but more $SrCO_3$ provides an environment for the generation of loosened carbon structure with larger BET surface area. The BET surface area significantly depends on the particle size and in general, smaller particle size corresponds to carbon products with higher BET surface area. In this manner, it is expected that carbon products with smaller particle size are acquired on increasing the $SrCO_3$ fraction.

A certain amount of $BaCO_3$ was previously utilized as a functional additive to stabilize the molten carbonate electrolyzer due to the lower Lewis basicity (the ability to donate a pair of electrons) of BaO than Li_2O, Na_2O and K_2O.[13,14,25] Herein, the SEM images of the carbon products electro-deposited in electrolyte with varying $BaCO_3$ fractions are displayed in Fig. 6. Amorphous carbon particles and carbon flakes were formed when 10% and 20% $BaCO_3$ were included in molten Li_2CO_3–Na_2CO_3–K_2CO_3 composite, as evident in Fig. 6a–d. When 30% $BaCO_3$ was dissolved in Li_2CO_3–Na_2CO_3–K_2CO_3 system, carbon products still presented amorphous microstructure (Fig. 6e), but a small amount of carbon nanotubes were observed, as marked with an arrow (Fig. 6f). The decomposition free energy of $BaCO_3$ into BaO and CO_2 is negative but higher than that of Li_2CO_3, Na_2CO_3 and K_2CO_3,[26] indicating that $BaCO_3$ degradation would proceed in a more facile manner. Moreover, the intermediate BaO originating from the $BaCO_3$ splitting shows a considerable advantage in dissolving into molten carbonates compared to alkali oxides.[14] The dissolved BaO tends to react with atmospheric CO_2 to form $BaCO_3$. Thus, it is thermodynamically concluded that the $BaCO_3$ additive demonstrates an even greater CO_2 absorption behavior than the Li_2CO_3–Na_2CO_3–K_2CO_3 matrix. The enhanced CO_2 dissolution promotes the carbonate regeneration process and facilitates compact carbon generation, resulting in a reduced BET surface area.

Carbon deposits formed in carbonate eutectic of Li_2CO_3–Na_2CO_3–K_2CO_3, Li_2CO_3–Na_2CO_3–K_2CO_3–$CaCO_3$ (30%), Li_2CO_3–Na_2CO_3–K_2CO_3–$SrCO_3$ (30%) and Li_2CO_3–Na_2CO_3–K_2CO_3–$BaCO_3$ (30%) are further studied by nitrogen adsorption–desorption automatic analysis. Nitrogen adsorption–desorption isotherm and pore size distribution are presented in Fig. 7a and b, respectively. Matching well with the BET surface area listed in Table 1, carbon products of Li_2CO_3–Na_2CO_3–K_2CO_3–$CaCO_3$ (30%) electrolysis show larger porosity than that of Li_2CO_3–Na_2CO_3–K_2CO_3 system, while those of 30% $SrCO_3$ and $BaCO_3$ additives, on the contrary, exhibit decreased porosity.

X-ray diffraction patterns of the carbon products of CO_2 dissolved in molten carbonates were recorded in order to develop a more profound understanding of the crystal structure, as presented in Fig. 7c–f. Both amorphous carbon and graphitic carbon consist of essentially parallel layer planes composed of several condensed benzene rings.[27,28] However, layer planes in amorphous carbons are randomly oriented rather than in an ordered arrangement, and

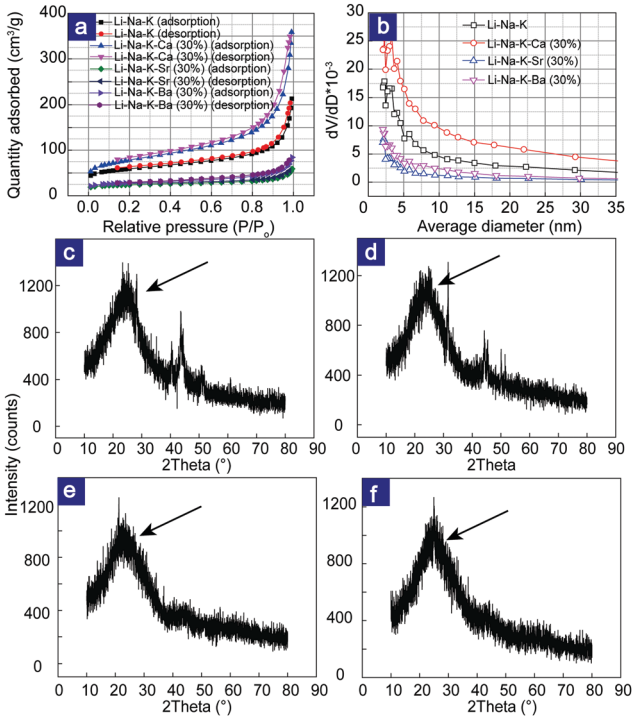

Fig. 7 Characterization of the carbon products. (a) Nitrogen adsorption–desorption isotherm. (b) Pore size distribution. (c–f) X-ray diffraction patterns of the carbon materials electro-deposited in Li_2CO_3–Na_2CO_3–K_2CO_3, Li_2CO_3–Na_2CO_3–K_2CO_3–$CaCO_3$ (30%), Li_2CO_3–Na_2CO_3–K_2CO_3–$SrCO_3$ (30%) and Li_2CO_3–Na_2CO_3–K_2CO_3–$BaCO_3$ (30%), respectively.

this defect leads to majority of the differences between amorphous carbon and graphitic carbon. Herein, a wide and weak carbon peak located at 26° is observed for the above carbon products, signifying that the CO_2-derived carbon products in the above four electrolytes are mostly amorphous. In contrast, on electrolyzing pure Li_2CO_3 at 723 °C, the cathodically generated carbon conformation is observed to produce carbon nanotubes in high yield and presents a sharp and enhanced carbon peak at 26° assigned to the well-ordered hexagonal graphite (002) diffraction planes within the carbon nanotubes.[29]

A visible difference in the carbon structure and BET surface area is presented on adding diverse alkaline earth carbonate with varying additive amounts. When alkaline earth carbonate was dissolved in the Li_2CO_3–Na_2CO_3–K_2CO_3 melts, the fluidity and conductivity of the molten salt system significantly changed. The former leads to an interface modification between the carbonate electrolyte and cathode. Carbon electro-deposition in the electrolyzer occurs on the cathodic surface, which is in reality significantly dependent on the interfacial interaction. Therefore, any minor change in the interface between the cathode and the electrolyte would provide the cathodically formed carbon products with different microstructures and BET surface areas. Moreover, the visible distinction of the cell voltages recorded during the galvanostatic electrolysis in varying electrolytes, which is induced by the changing conductivity as alkaline earth carbonate additives are included, provides different carbon deposition rates. This would also impact the microstructure of the carbon products to some extent. As further demonstrated herein, $BaCO_3$ and $SrCO_3$ additives generate compact carbon structures with lower BET surface areas than Li_2CO_3–Na_2CO_3–K_2CO_3 melts. For $CaCO_3$, low $CaCO_3$ fraction deposits carbon products with compact microstructure, while sufficient amount would preferably lead to loosened carbon structure production with larger BET surface area than that obtained in the Li_2CO_3–Na_2CO_3–K_2CO_3 system. It was previously measured that the solubility of CaO in molten carbonates was 30 to 100 times less than that of $CaCO_3$ and 50 times less than that of Li_2O.[30] Hence, the interesting influence of $CaCO_3$ on the carbon production is believed to be mainly caused by the poor solubility of CaO in molten carbonates.

Carbon nanotubes, instead of amorphous carbons, were deposited by optimizing the electrolytic conditions. A nickel wire disk with an area of 10 cm^2 and a galvanized iron wire disk with an area of 5 cm^2 were employed as the anode and cathode, respectively. A 50 mL-corundum crucible served as the electrolytic container in this study rather than the previously reported nickel crucible.[11,29] In the latter case, the inner wall of the nickel crucible acted as the anode simultaneously, and no additional nickel anode was employed. Li_2CO_3 melts at 723 °C and to ensure good fluidity, pure Li_2CO_3 electrolysis was also carried out at over 730 °C. Herein, we performed the pure Li_2CO_3 electrolysis at 730 °C, 750 °C and 770 °C, as depicted in Fig. 8a–c, respectively. Evidently, the pure Li_2CO_3 electrolysis generates a high yield of carbon nanotubes with an external diameter of ~100 nm and an inner diameter of merely tens of nanometers. The length of the carbon nanotubes subsequent to pure Li_2CO_3 electrolysis varies from tens of microns to hundreds of microns. No visible change in the diameter of the synthetic carbon nanotubes is observed along with the increase in electrolytic temperature.

Preparation of carbon nanotubes in $CaCO_3$-, $SrCO_3$- and $BaCO_3$-included molten Li_2CO_3 were performed at 750 °C, as presented in Fig. 8d–f, respectively. Compared to that of pure Li_2CO_3 electrolysis, alkaline earth carbonate additives provide thicker carbon nanotube structure. The increase in the diameter of the carbon nanotube structure is presumably because of the interface modification induced by the alkaline earth carbonate additives. An additional observation from the TEM images is that the carbon nanotubes of pure Li_2CO_3 present a very small inner void, while a more prominent hollow structure is observed when alkaline earth carbonate is added into molten Li_2CO_3. In fact, the carbon nanotubes subsequent to pure Li_2CO_3 electrolysis were once considered as solid carbon nanofibers until TEM characterization was employed.[29,31] The selective synthesis of carbon nanotubes and carbon nanofibers could be achieved through isotopic labeling, where $^{13}CO_2$ favors a straightforward synthesis of carbon nanofibers and naturally abundant $^{12}CO_2$ facilitates hollow carbon nanotubes production.[31]

The formation mechanism of carbon nanotubes in molten carbonate environment is attributed to the nucleating effect of nickel nanoparticles deriving from the reduction and redeposition of dissolved nickel oxide. To deposit high quality uniform carbon nanotubes, an initial low current step is required in order to

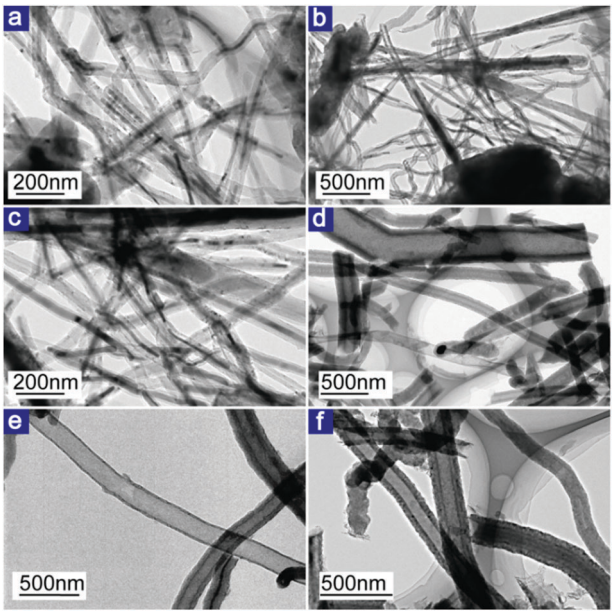

Fig. 8 Carbon nanotubes prepared in pure Li_2CO_3 at (a) 730 °C, (b) 750 °C and (c) 770 °C. Carbon nanotubes prepared in 750 °C alkaline-earth-carbonate-included electrolyte (d) Li_2CO_3–$CaCO_3$, (e) Li_2CO_3–$SrCO_3$ and (f) Li_2CO_3–$BaCO_3$.

deoxidize of nickel oxide. In this case, before using 200 mA cm^{-2} to obtain a rapid carbon nanotube deposition, current densities of 6 mA cm^{-2}, 10 mA cm^{-2} and 20 mA cm^{-2} were initially applied to the electrolyzer for 15 min, 15 min and 5 min, respectively, to grow nickel nucleation sites on the cathodic surface controllably. During this process, cell voltage increased from ~0.8 V to ~1.05 V, which was sufficient to reduce nickel oxide to form nickel nanoparticles but insufficient for carbon deposition. Zinc metal is another essential factor for carbon nanotubes growth, but acts in a different manner from nickel anode. In the absence of zinc but in the presence of nickel, CO_2 electrolysis produces amorphous carbon graphite and uncontrolled nanofiber structures with circular or rectangular duct-like cross sections. In contrast, when nickel rather than galvanized iron is used as the cathode and ZnO (1% by wt) is added directly into the electrolyte, the nickel crucible electrolysis still nucleates high-yield and high-quality carbon nanotubes.[11]

The diameter of a nanotube significantly affects its mechanical and electronic properties and thus can influence its performance in a variety of applications.[32–35] Herein, it is verified that the electrolysis using alkaline earth carbonate additives provides thicker carbon nanotubes production compared to the pure Li_2CO_3 electrolysis. Additionally, we compare the carbon nanotubes formed in the Li_2CO_3 electrolyte presented in this work and previous reports,[11,29] as listed in Table 2. It is demonstrated that besides the inclusion of the alkaline earth carbonate, the electrolytic container and electrolysis duration would also impact the carbon nanotubes deposition. The nickel crucible electrolysis was observed to deposit carbon nanotubes at a high yield, but the carbon nanotubes exhibit wider diameter of 200–300 nm.[29] In ref. 29, the inner wall of the nickel container was utilized as the anode and provided larger active area than the 10 cm^2 nickel wire disk. The increase in anode area may facilitate nickel release and form larger transitional metal nucleation sites, providing the carbon nanotubes with larger diameter. As further reported in ref. 11, extended electrolysis duration generates proportionally thicker carbon nanotubes due to the continuous carbon deposition, which in turn signifies the excellent regeneration of the carbonates electrolyte.

Table 2 Comparison of the external diameter of the carbon nanotubes in the literature

Container	Duration/min	External diameter/nm	Ref.
Corundum crucible	≤120	100	This work
Nickel crucible	≤120	200–300	29
Nickel crucible	1200	2500	11

Conclusions

In this study, the conversion of CO_2 into carbon fuel or even valuable carbon nanotubes was achieved *via* electrolysis in alkaline-earth-carbonate-included carbonate eutectic. The reduction of tetravalent carbonate ions to zerovalent solid carbon occurs on the cathode surface and significantly depends on the interfacial interaction. Li_2CO_3–Na_2CO_3–K_2CO_3 electrolysis without dissolving the alkaline earth carbonate generates a carbon product with a porous, honeycomb-like structure. The addition of $CaCO_3$, $SrCO_3$ and $BaCO_3$ leads to a significant change in the carbon morphology, from a porous, honeycomb-like carbon to a mixture of carbon flakes, sphere-like carbons and irregular carbon particles. The morphological evolution after the addition of diverse alkaline earth carbonates by varying amounts is mainly due to the interface modification between the cathode and the carbonates electrolyte. Moreover, $SrCO_3$ and $BaCO_3$ additives provide a lower BET surface area than the carbon products of Li_2CO_3–Na_2CO_3–K_2CO_3, while sufficient $CaCO_3$ endows the carbon products with a larger BET surface area than Li_2CO_3–Na_2CO_3–K_2CO_3 (264 m^2 g^{-1} *vs.* 193 m^2 g^{-1}), which could be attributed to the formation of the nearly insoluble intermediate CaO. The XRD patterns signify that the synthesized carbon products are of low crystallinity due to the random order of the layer planes. Moreover, the carbon product of CO_2 dissolved in over 700 °C Li_2CO_3–$CaCO_3$, Li_2CO_3–$SrCO_3$ and Li_2CO_3–$BaCO_3$ is seen to produce valuable carbon nanotubes in high yield. This suggests that carbon nanotubes synthesis could be fulfilled in a more economic electrolyte rather than with rare and expensive pure Li_2CO_3. Summarily, the alkaline-earth-carbonate-included molten carbonates electrolyzer could sustain continuous CO_2 electrolysis and carbon electro-deposition, providing a new alternative electrolyte component to consume unwanted CO_2 greenhouse gas and generate reusable carbon products.

Conflicts of interest

There are no conflicts of interest to declare.

Acknowledgements

This study was supported by the National Natural Science Foundation of China (21476046, 21306022 and 21808030), the Science Fund for Distinguished Young Scholars of the Heilongjiang Province of China (JC2017002), the Natural Science Foundation of Heilongjiang Province (E2018014), the Postdoctoral Launch Fund of the Heilongjiang Province of China (LBH-Q17033) and Northeast Petroleum University (KYCXTD201703, 2017PYQZL-07 and JYCX_CX03_2018).

Notes and references

1 F. Johnsson, *Greenhouse Gases: Sci. Technol.*, 2011, **1**, 119–133.
2 B. Mai, C. S. Adjiman, A. Bardow, E. J. Anthony, A. Boston, S. Brown, P. S. Fennell, S. Fuss, A. Galindo and L. A. Hackett, *et al.*, *Energy Environ. Sci.*, 2018, **11**, 1062–1176.
3 M. Mikkelsen, *Energy Environ. Sci.*, 2010, **3**, 43–81.
4 Y. K. Delimarskii, O. V. Gorodiskii and V. F. Grishchenko, *Dokl. Akad. Nauk SSSR*, 1964, **156**, 650–651.
5 M. D. Ingram, B. Baron and G. J. Janz, *Electrochim. Acta*, 1966, **11**, 1629–1639.
6 H. V. Ijije, R. C. Lawrence, N. J. Siambun, S. M. Jeong, D. A. Jewell, D. Hu and G. Z. Chen, *Faraday Discuss.*, 2014, **172**, 105–116.
7 H. Ijije, R. Lawrence and G. Chen, *RSC Adv.*, 2014, **4**, 35808–35817.
8 V. Kaplan, E. Wachtel, K. Gartsman, Y. Feldman and I. Lubomirsky, *J. Electrochem. Soc.*, 2010, **157**, B552–B556.
9 H. V. Ijije and G. Z. Chen, *Adv. Manuf.*, 2016, **4**, 23–32.
10 H. V. Ijije, C. Sun and G. Z. Chen, *Carbon*, 2014, **73**, 163–174.
11 H. Wu, Z. Li, D. Ji, Y. Liu, L. Li, D. Yuan, Z. Zhang, J. Ren, M. Lefler and B. Wang, *et al.*, *Carbon*, 2016, **106**, 208–217.
12 L. Massot, P. Chamelot and F. Bouyer, *Electrochim. Acta*, 2002, **47**, 1949–1957.
13 Y. Yu, Z. Li, W. Zhang, W. Li, D. Ji, Y. Liu, Z. He and H. Wu, *New J. Chem.*, 2018, **42**, 1208–1215.
14 S. Licht, B. Cui and B. Wang, *J. CO2 Util.*, 2013, **2**, 58–63.
15 S. Licht, *J. Phys. Chem. C*, 2009, **113**, 16283–16292.
16 S. Licht, B. Wang, S. Ghosh, H. Ayub, D. Jiang and J. Ganley, *J. Phys. Chem. Lett.*, 2010, **1**, 2363–2368.
17 Z. Li, D. Yuan, H. Wu, W. Li and D. Gu, *Inorg. Chem. Front.*, 2018, **5**, 208–216.
18 D. Tang, H. Yin, X. Mao, W. Xiao and D. H. Wang, *Electrochim. Acta*, 2013, **114**, 567–573.
19 P. Ramesh and S. Sampath, *Anal. Chem.*, 2003, **75**, 6949–6957.
20 F. Gao, X. Guo, J. Yin, D. Zhao, M. Li and L. Wang, *RSC Adv.*, 2011, **1**, 1301–1309.
21 H. Yin, X. Mao, D. Tang, W. Xiao, L. Xing, H. Zhu, D. Wang and D. R. Sadoway, *Energy Environ. Sci.*, 2013, **6**, 1538–1545.
22 S. Licht, B. Wang and H. Wu, *J. Phys. Chem. C*, 2011, **115**, 11803–11821.
23 G. Sneddon, A. Greenaway and H. H. P. Yiu, *Adv. Energy Mater.*, 2014, **4**, 281–286.
24 H. Wu, Z. Li, D. Ji, Y. Liu, G. Yi, D. Yuan, B. Wang and Z. Zhang, *RSC Adv.*, 2017, **7**, 8467–8473.
25 F. F. Li, S. Liu, B. Cui, J. Lau, J. Stuart, B. Wang and S. Licht, *Adv. Energy Mater.*, 2015, **5**, 76–78.
26 J. Ren, J. Lau, M. Lefler and S. Licht, *J. Phys. Chem. C*, 2015, **119**, 23342–23349.
27 K. L. Saenger, J. C. Tsang, A. A. Bol, J. O. Chu, A. Grill and C. Lavoie, *Appl. Phys. Lett.*, 2010, **96**, 153105.
28 T. Kim, J. Lee and K. H. Lee, *RSC Adv.*, 2016, **6**, 24667–24674.
29 J. Ren, F. F. Li, J. Lau, L. González-urbina and S. Licht, *Nano Lett.*, 2015, **15**, 6142–6148.
30 S. Licht, H. Wu, C. Hettige, B. Wang, J. Asercion, J. Lau and J. Stuart, *Chem. Commun.*, 2012, **48**, 6019–6021.
31 J. Ren and S. Licht, *Sci. Rep.*, 2016, **6**, 27760.
32 M. F. De Volder, S. H. Tawfick, R. H. Baughman and A. J. Hart, *Science*, 2013, **339**, 535–539.
33 C. L. Cheung, A. Kurtz, H. Park and C. M. Lieber, *J. Phys. Chem. B*, 2002, **106**, 2429–2433.
34 S. Kang, M. Herzberg, D. F. Rodrigues and M. Elimelech, *Langmuir*, 2008, **24**, 6409–6413.
35 M. Zheng, A. Jagota, M. S. Strano, A. P. Santos, P. Barone, S. G. Chou, B. A. Diner, M. S. Dresselhaus, R. S. McLean and G. Onoa, *et al.*, *Science*, 2003, **302**, 1545–1548.

